SCIENTIFIC PAPER

Numerical simulation on the processing of crumb rubber modified asphalt by ultrasound and mechanical stirring

Gang Fu[1], Ruien Yu[1,2,*], Xiaolin Yu[1], Xiaohan Li[1], Xiaowen Chen[3], Xiaoyan Zhang[2], Yanfei Kou[1], Xijing Zhu[1]

[1]Shanxi Key Laboratory of Advanced Manufacturing Technology, North University of China, Taiyuan 030051, China;
[2]Shanxi Transportation Technology Research & Development Co., Ltd, Taiyuan 030032, China;
[3]State Key Laboratory of Special Functional Waterproof Materials, Beijing Oriental Yuhong Waterproof Technology Co., Ltd, Beijing 101100, China

https://doi.org/10.2298/CICEQ230724008F

Received 24.7.2023.
Revised 29.2.2024.
Accepted 6.3.2024.

* Correspondence: Ruien Yu, Shanxi Key Laboratory of Advanced Manufacturing Technology, North University of China, Taiyuan 030051, China.
Email: yuruien@nuc.edu.cn

Abstract: Based on the existing modified asphalt production equipment, the power ultrasonic is integrated into the existing stirring dispersion technology, and the FLUENT fluid simulation is used to combine ultrasonic and stirring. Stirring and ultrasonic two motion forms were realized step by step, and the movement states of crumb rubber modified asphalt were simulated under the interaction of ultrasonic and stirring, which provide a new method for the research of crumb rubber modified asphalt production equipment. The results show that under the action of ultrasound, only positive pressure exists in the modified asphalt flow field after adding the cavitation model, and the maximum absolute pressure can reach about 1200kPa. With the increase of ultrasonic time, the air content rate under the tool head is periodic and regular changed and will gradually increase, the number of cavitation bubbles will continue to increase, and the cavitation intensity will increase. The influence of asphalt viscosity on the volume fraction of cavitation bubbles was studied, when the viscosity of the system is 0.8 Pa·s, it is more conducive to the occurrence of cavitation, The process of ultrasonic synergistic stirring is conducive to inhibiting the segregation phenomenon of crumb rubber modified asphalt.
Keyword: Ultrasound; Cavitation; Crumb rubber modified asphalt; Mechanical stirring; CFD simulation

Article Highlights

- Fluid simulation of modified asphalt is conducted under ultrasound and stirring processing.
- The cavitation volume fraction in the tank changes periodically with the ultrasound effect.
- The cavitation strength of modified asphalt is compared in the different system viscosities.

Introduction

Asphalt is one of the indispensable materials in the process of expressway construction. Due to various reasons such as the increase in traffic volume and global warming, base asphalt cannot meet the needs of expressway construction [1,2], polymer modification is currently one of the most common methods to improve the performance of asphalt, and polymer modified asphalt has been widely used in road construction [3-6]. With the increase in the number of cars in the world, waste tires as a new "black pollution", its number is also increasing, the waste tires broken into crumb rubber as a modifier added to the asphalt, not only can reduce the production cost of modified asphalt, but also to achieve waste utilization, green development [7-8].

At present, the modification of base asphalt is mainly based on the addition of one or more polymers. Ameri et al. [9] studied the effect of EVA content on the storage stability of asphalt and found that the greater the amount of EVA in asphalt, the greater the degree of segregation. Xiao et al. [10] analyzed the rheological properties of the modified asphalt binder with crumb rubber added at high temperature, and the results showed that the rheological properties of the modified binder depend on the polymer type and asphalt source. Liu et al. [11] tested the conventional performance, rheological properties and infrared spectroscopy test analysis, found that APAO can greatly improve the anti-aging performance of asphalt. Jiang et al. [12] prepared epoxy SBS-modified asphalt and found that the properties of epoxy SBS-modified asphalt depended on the ratio of S/B, the compatibility of SBS and asphalt, the average molecular weight of SBS, and the dispersion of SBS-modified asphalt particles in the continuous epoxy phase. Leng et al. [13] conducted experimental studies on composite WTR (waste tire rubber) and waste PE (polyethylene) or PET (polyethylene terephthalate) modified asphalt, and the experimental results proved that the composite modified asphalt improved the performance of rutting deformation. Ding et al. [14] compared the performance of ordinary asphalt recycled material and SCRA recycled asphalt mixture, and found that the low temperature performance of SCRA recycled asphalt mixture could be further improved, while other properties remained at a high level. By studying the foaming conditions of FWMA-CR binder and combining with the performance evaluation of FWMA-CR binder and mixture, Hu et al. [15] found that compared with the hot-mix asphalt mixture containing rubber debris

(HMA-CR), the manufacturing temperature of FWMA-CR mixture dropped by 17°C. The foamed rubber asphalt binders and mixtures showed better low temperature performance and fatigue resistance, but poor high performance.

Li et al. [16] adopted the orthogonal experimental design method and found that when 2% nano-montmorillonite and 8% SBS were cut for 150min at a shear temperature of 170℃ and a shear rate of 4000 rpm, the modified asphalt with a high content of SBS had good high and low temperature performance and the best compatibility. Traditional methods by adding surfactants, compatibilizers, stabilizers and other chemical reagents to promote the compatibility of the two phases and the stability of the blending system, but chemical reagents are not conducive to clean production, and although the performance of asphalt can be improved by adding modifier, but with the extension of storage time, the modified asphalt will also appear segregation, aging and other phenomena. As a result, the quality of modified asphalt decreases [17-21], so it is necessary to adopt new technology, new technology and interdisciplinary research on polymer modified asphalt blending system. Xiong et al. [22] adopted a thermochemical mechanics method to efficiently transform polypropylene (PP) waste into maleated epoxidation degradation products through the hybridization of diisopropyl benzene peroxide (DCP), maleic anhydride (MAH) and epoxy soybean oil (ESO), which was used as warm mixed asphalt modifier (PPMs) to achieve better modification effects and enhanced properties. Wang et al. [22] abandoned the traditional shear method, and the modified asphalt prepared by the twin-screw shear method had better storage stability and low temperature performance than the modified asphalt prepared by the traditional shear method. Loderer et al. [23] produced rubber particles with a coarser and larger surface area using high-pressure water jet technology, and crumb rubber modified asphalt produced from such rubber particles has better low-temperature ductility.

Among many emerging technologies, ultrasonic processing offers the advantages of efficiency and cleanliness [24-26]. Studies have shown that the cavitation effect generated by ultrasound can enhance the stirring effect on the system and refine the polymer particles [27]. The research of ultrasonic in the field of asphalt and crude oil has also been widely used, and the high temperature and high pressure environment generated by ultrasonic cavitation can change the position of weak bond energy in asphalt, thereby promoting the chemical reaction

during the development of modified asphalt [28]. Many scholars have applied ultrasound to the research of asphalt and crude oil, and studied the influence of ultrasound on it. Based on the effects of ultrasonic cavitation on asphaltene content, rheological properties and metal content under different ultrasonic frequency and power input conditions, the results of Mohapatra and Kirpalani [29] show that under specific ultrasonic frequencies and powers, the strong attraction phase interaction between asphalt particles decreases, resulting in a decrease in asphalt viscosity, which improves the transportation performance of asphalt. Razavifar and Qajar [30] studied the effect of ultrasonic irradiation on the viscosity and thermal behavior of crude oil with high asphaltene content under different irradiation time and power/frequency, the reduction in oil viscosity is even greater. Mousavi et al. [31] studied the effect of ultrasonic waves on crude oil, and found that ultrasonic waves would decompose asphaltenes in crude oil, reducing the viscosity of asphalt and changing the rheology of asphalt. Based on the viscosity-temperature characteristics of asphalt, Wang et al. [32] analyzed the viscosity change trend of molten asphalt in the ultrasonic treatment test, the results show that the cyclic vibration and cavitation effect generated by ultrasonic irradiation can effectively reduce the viscosity of asphalt, thereby enhancing the flow at high temperature.

Although ultrasonic technology has been applied in the field of asphalt research such as viscosity reduction and desulfurization, it is still difficult to apply ultrasonic in actual industrial production, Therefore, based on the modification process of stirring and ultrasound on asphalt, the combined effect of stirring and ultrasound on polymer-modified asphalt is numerically simulated, By analyzing the fluid motion state, velocity and pressure in the tank under the joint action of ultrasonic and mechanical stirring, the feasibility of ultrasonic and mechanical stirring on asphalt modification was studied. Through the parameters of the simulation model and the simulation results, the theoretical foundation for the further optimization of the ultrasonic stirring equipment of polymer-modified asphalt is laid.

Numerical Simulation and Simulation Methods

Construction of the simulation domain

The tanks used in the study are cylindrical, and the agitator is a six-blade disc stirrer, as shown in Fig.1(a). Deepen the tool head into the tank, and ensure that there is a certain distance

between the agitator and the tool head. The CFD fluid calculation software is used for the numerical simulation of ultrasonic action on polymer modified asphalt. During the simulation process, the model is simplified to a certain extent, and the multiple reference system method is used to establish the model. The simplified model diagram of the combination of various parts is shown in Fig.1 (b).

Fig.1

Construction of the numerical models

According to the three laws followed by fluid mechanics, the law of conservation of mass, momentum and energy, mathematical models are established, namely continuity equation, momentum conservation equation and energy conservation equation.

(1) Law of conservation of mass

According to the law of conservation of mass, the difference between the inflowing mass and the outflowing mass of the fluid microelement in unit time is equal to the increment of the fluid mass inside the fluid microelement. When the liquid is incompressible, i.e. the density is unchanged, its expression is as in Equation (1).

$$\frac{\partial u}{\partial x}+\frac{\partial v}{\partial y}+\frac{\partial w}{\partial z}=0 \tag{1}$$

Where u, v, w are the components of velocity vector $\boldsymbol{u}$ on x, y, z respectively.

(2) The momentum equation

The momentum equation is also called the Navier-Stokes equation, which is expressed as the rate of change of the microelement fluid over time equal to the sum of all the forces acting on the microbody externally, and the equations for conservation of momentum in the three directions of three-dimensional space *x, y, z* are as follows.

$$\frac{\partial(\rho u)}{\partial t}+div(\rho uU)=div(ugradu)-\frac{\partial P}{\partial x}+S_u \tag{2}$$

$$\frac{\partial(\rho v)}{\partial t}+div(\rho vU)=div(ugradv)-\frac{\partial P}{\partial y}+S_v \tag{3}$$

$$\frac{\partial(\rho w)}{\partial t}+div(\rho wU)=div(ugradw)-\frac{\partial P}{\partial z}+S_w \tag{4}$$

Among them, the three relational expressions of S_u, S_v, and S_w are as follows.

$$S_u = \frac{\partial}{\partial x}(\mu\frac{\partial u}{\partial x}) + \frac{\partial}{\partial y}(\mu\frac{\partial v}{\partial x}) + \frac{\partial}{\partial z}(\mu\frac{\partial w}{\partial x}) + \frac{\partial}{\partial x}(\lambda divU) \tag{5}$$

$$S_u = \frac{\partial}{\partial x}(\mu\frac{\partial u}{\partial x}) + \frac{\partial}{\partial y}(\mu\frac{\partial v}{\partial x}) + \frac{\partial}{\partial z}(\mu\frac{\partial w}{\partial x}) + \frac{\partial}{\partial x}(\lambda divU) \tag{6}$$

$$S_u = \frac{\partial}{\partial x}(\mu\frac{\partial u}{\partial x}) + \frac{\partial}{\partial y}(\mu\frac{\partial v}{\partial x}) + \frac{\partial}{\partial z}(\mu\frac{\partial w}{\partial x}) + \frac{\partial}{\partial x}(\lambda divU) \tag{7}$$

Where μ is the dynamic viscosity and λ is the second molecular viscosity.

(3) Law of conservation of energy

For the flow system in the tank, the law of energy conservation is satisfied. This definition can be described as the increase in energy in the microbody is equal to the sum of the net heat flux into the microbody and the work done by physical and surface forces on the microbody, and the expression is as follows.

$$\frac{\partial(\rho T)}{\partial t} + \nabla(\rho u T) = \nabla\left(\frac{k}{C_p}\cdot grad\left(T\right) + S_t\right) \tag{8}$$

where T is the temperature, k is the heat transfer coefficient of the fluid, C_p is the specific heat capacity and S_t is viscous dissipation term.

Grid division

The established model is imported into ICEM in STP format for meshing, in the process of meshing, the agitator and the nearby area and other areas are separated, the agitator and the nearby area are the moving area, other areas are static area, the liquid flow speed near the agitator is significantly higher than other areas, the flow field form is the most complex, therefore, it is divided by a structured grid, the grid of the moving area is refined, the grid of the static area can be slightly thicker, which can not only improve the calculation accuracy, but also shorten the calculation time, the grid quality requirement is higher than 0.6, and the number of grids is about 1.2 million.

Initial and Boundary Conditions

The fluid simulation is a simulation of liquid-gas mixing, the mixture model is adopted, the main phase is modified asphalt, the secondary phase is air, the wall of the tank with the tool

head is the pressure outlet, the air is allowed to enter and exit freely, and the wall model adopts the scable wall function.

The wall thickness is set to 2 mm, and the temperature of the entire tank is set to 120°C to ensure that the asphalt is in a liquid state. The density of the crumb rubber modified asphalt used is 1.0 g/cm^3, and the viscosity is 1.2 Pa·s. The high-order differential solution format is selected for numerical calculation, and the iterative residual convergence accuracy is 1×10^{-6}. The reference pressure is the standard atmospheric pressure, the acceleration of gravity is 9.81 m/s^2, the direction is negative, the implicit separation algorithm is used, the wall surface adopts the no-slip wall boundary condition, the density-based solution method is adopted, the turbulence model selects the 1 model, and the speed-pressure coupling adopts the SIMPLE algorithm.

For the condition setting of ultrasonic cavitation, the end face of the tool head is the motion boundary. According to the working parameters of the ultrasonic generator, the displacement equation for setting the boundary of motion is equation (9).

$$x = A\sin(2\pi ft) \tag{9}$$

Where A is the amplitude, and f is the frequency of the ultrasonic transducer.

By deriving it, the vibration velocity equation of the end face of the tool head is equation (10).

$$V = 2\pi f \times A \times \cos(2\pi ft) \tag{10}$$

Equation (10) is compiled into a moving grid boundary by a UDF program.

Model validation

Due to the large difference between the frequency of ultrasonic vibration and the rotation speed of the agitator, the agitator is rotated first, and then the ultrasonic vibration simulation was performed. In order to check a good and appropriate setting of the boundary conditions, as well as the chosen computational mesh, a rough simulation was performed first. The speed of the agitator was set at 300rpm, the iteration time step was 0.01s, and the iteration was 200 times, and the velocity field distribution in the tank was obtained, as shown in Fig.2. It can be seen from the figure that the velocity is large in the region close to the agitator, relatively small in the region far away from the agitator, and almost zero in the region close to the boundary of the

tool head. The flow pattern generated by the six straight blade turbine agitator is mainly radial flow. The radial flow generated by the rotation of the blades drives the crumb rubber modified asphalt to flow to the edge of the tank. After the fluid hits the wall, it is divided into two parts, one part moves downward, and the other part moving upward, the fluid moving downward meets the lower wall and flows to the stirring shaft, and then returns to the blade area. Due to the inhibition of the tool head, the fluid moving upwards only forms a backflow area between the tool head and the wall, while the liquid below the tool head has almost no fluid movement, and a dead zone will appear in this area. The dead zone does not exist at first, as the fluid continues to move, until the motion area expands to cover the bottom surface of the tool head, the dead zone begins to appear, and then this area begins to expand, until the fluid in the entire tank begins to move, the dead zone occupies the maximum area, and then iteratively enters the next cycle, and the dead zone area begins to decrease again. When the stirrer rotates to 2s, that is, the stirrer stirs 10 laps at this time, and basically reaches a steady state.

Fig.2

Results and discussion

Asphalt movement in the mixing tank

The amplitude of the tool head is 10 μm, the vibration frequency is 20 kHz, the time step is set to 1×10^{-7} s, and the iteration is 1500 steps, which is three cycles. Data is recorded every 10 steps, and a point is taken on the tool head, the speed of movement at this point is shown in Fig.3(a). It can be seen that the tool head has no vibration in the first 200 steps, and the speed is 0. The agitator in the tank is given a rotating speed of 300 rpm, and under the action of the agitator, the modified asphalt starts to rotate around the axis. The modified asphalt gradually diffuses outward from the initial rotation, and at 2s, the modified asphalt in the entire tank basically moves and forming a circulating field.

After adding the vibration and cavitation model of the tool head, the speed in the tank changes. According to the monitored speed, it can be seen that from step 240 to step 740 is a complete cycle. From 240 steps, the speed of the tool head gradually begins to increase, the tool head is in the lowest point position, and starts the movement upwards, at this time, the modified

asphalt under the tool head has a certain movement speed due to the compression of the tool head in the previous cycle, and the movement of the modified asphalt far away from the tool head basically has little effect, it is still dominated by stirring movement. Fig.3(b) shows the velocity of asphalt in the tank when iterating step 440. At this time, the velocity of the tool head reaches a maximum of 1.279 m/s, and the movement speed of the tool head gradually decreases when the iteration continues. When the tool head moves to the highest point, the speed decreases to 0. From then on, the tool head will move down to the lowest point, and start the next cycle of motion at the same time. This reciprocating motion forms high-frequency vibrations of the tool head. The main influence range of ultrasonic is near the end face of the tool head, and the movement of other areas is mainly affected by stirring, and the asphalt inside the tank can flow through the action of stirring, and then ultrasonic has an effect on the asphalt in the entire tank.

Fig.3

Pressure distribution in the mixing tank

First, the UDF-compiled program is loaded into the model, the cavitation model is closed and the agitator stops stirring, and the pressure change is observed to obtain the pressure cloud at high pressure as shown in Fig.4(a). It can be seen from the figure that there is a high pressure under the tool head, which diffuses outward and gradually decreases. Under the action of ultrasound with an amplitude of 10 μm and a vibration frequency of 20 kHz, its application range is mainly in a small range under the tool head. When the same cycle changes, negative pressure will also occur at this position, and negative pressure will make the internal pressure of asphalt lower than the saturated vapor pressure, and cavitation will occur under the action of alternating positive and negative pressure.

Fig.4

Under the action of mechanical vibration and cavitation of the tool head, the maximum value of the absolute pressure in the tank in three cycles changes with the iteration time as shown in Fig. 4(b). It can be seen from the figure that the absolute pressure inside the container is positive pressure. In the first 200 steps, there is only stirring in the tank. The maximum pressure in the asphalt is about 100kPa, which is the standard atmospheric pressure. Cavitation

does not occur. From step 200 to step 1700, the speed of the tool head presents a trend of sinusoidal motion, which conforms to the characteristics of the vibration cycle. The addition of ultrasonic vibration causes the fluid velocity to change, and under the effect of cavitation, the absolute pressure inside the liquid changes. After applying the ultrasonic vibration model from 2s, the sudden change in pressure from 100 kPa to 390 kPa is due to the change in speed. With the beginning of the iteration, the absolute pressure inside the liquid increases rapidly until it reaches the peak value of about 1100 kPa when the iteration reaches step 510, and then drops rapidly. When the iteration reaches step 640, the absolute pressure returns to 220 kPa, and the iteration continues, the maximum absolute pressure change presents a periodic change, which is consistent with the periodic characteristics of tool head vibration.

Starting from step 240, the absolute pressure diagram in the tank is taken every 50 steps until step 740, as shown in Fig.6. At step 240, the ultrasonic tool head is at the lowest point, and the absolute pressure is shown in Fig. 5(a). At this time, the speed of the tool head is 0, and the overall absolute pressure in the tank is very low. The absolute pressure is close to 0 below the tool head, and the maximum pressure is caused by stirring, which is at the same level as the agitator and far from the tool head. At step 340, the tool head is close to the equilibrium position, and the absolute pressure is shown in Fig.5(b). At this time, the absolute pressure in the tank does not change much, and the maximum absolute pressure is at the edge of the tool head. This is due to the different flow direction of the asphalt under the tool head and on the side, where the side asphalt rotates around the tool head, while the asphalt below the tool head moves up and down, resulting in a relatively high pressure here. At step 440, as shown in Fig. 5(c), the tool head has crossed the equilibrium position and is close to the highest point. At this time, the absolute pressure near the tool head changes, and the absolute pressure in the tank can reach a maximum of 550 kPa, its value rises significantly, and the absolute pressure changes greatly. At step 540, as shown in Fig. 5(d), the absolute pressure at the tool head reaches 1140 kPa. At this time, the tool head moves from the highest point position to the equilibrium position, and the cavitation volume fraction generated at this time basically reaches near the first peak, and the cavitation intensity is large. The absolute pressure value under the tool head is stable at 1100 kPa from step 500 to step 560. At step 640, the absolute pressure is shown in Fig. 5(e). The tool head has just crossed the equilibrium position and moved to the lowest position, and its value

basically drops to 225 kPa, which is not much different from the step 240 at the beginning of the above. The position under the tool head first weakens in the middle, then weakens on both sides. At this time, the cavitation intensity decreases, but it is the first inflection point of the gas fraction change, and then the gas fraction will gradually increase. At step 740, the absolute pressure is shown in Fig. 5(f). The tool head has reached the lowest point, and the absolute pressure below the tool head returns to 220 kPa, which is basically the same as at step 240, indicating that the absolute pressure change conforms to the periodic law. Continue iterating to start the cycle of the next cycle. However, the pressure is not consistent away from the tool head, because the absolute pressure distribution is different due to the agitator rotation. To sum up, it can be seen that within a cycle, the increase of the absolute pressure change under the tool head mainly occurs between step 430 and 500, the peak absolute pressure is stable between step 500 and step 560, and the decrease occurs between step 560 and step 630. The absolute pressure changes are very small except under the tool head, so the position of ultrasonic cavitation is mainly directly under the tool head, and the cavitation area is small.

Fig.5

Change of gas volume fraction in the mixing tank

Taking the maximum volume fraction of cavitation bubbles in the tank as the research object, the maximum change of the volume fraction of cavitation bubbles in the tank is shown in Fig. 6(a). Before step 200, the volume fraction of cavitation bubbles in the tank is 0, and there is only stirring in the tank during this time, so no cavitation occurs and no cavitation bubbles are generated. From step 200, the maximum volume fraction of cavitation bubbles in the tank began to increase, indicating that cavitation reactions began to occur. At step 470, the maximum volume fraction of cavitation bubbles reaches the first inflection point, at which time the cavitation bubble volume fraction is 0.36%, the cavitation intensity reaches the maximum in the first cycle, and then the volume fraction of cavitation bubbles begins to decrease. The second inflection point is reached at step 580, when the volume fraction is 0.29%, the cavitation intensity decreases slightly compared to before, and then the cavitation bubble volume fraction begins to rise again, starting the next cycle of changes. Comparing the volume fraction of cavitation bubbles in the three cycles, the volume fraction of cavitation bubbles in the latter

cycle increases compared with the previous cycle, indicating that cavitation bubbles continue to increase under the action of ultrasound, and the positive and negative pressures in each cycle continue to change, so that the cavitation bubbles have periodic growth, showing a trend of steady-state cavitation.

According to the distribution of cavitation bubbles in the cavitation process, the volume fraction of cavitation bubbles in the third cycle is the largest, that is, at step 1490, and the cavitation bubbles distribution in the tank is shown in Fig. 6(b). It can be seen from the figure that the generation of cavitation bubbles is mainly concentrated directly below the tool head. The closer to the tool head, the larger the volume fraction of cavitation bubbles and the higher the cavitation intensity. However, the range of cavitation bubbles is very small, and the asphalt in the entire tank can be driven by stirring, and finally the asphalt in the entire tank is subjected to ultrasound.

Fig. 6

Effect of viscosity on simulation results

Asphalt is a temperature-sensitive material, when the temperature rises or falls, its viscosity changes greatly. Therefore, Therefore, the ultrasonic simulation of asphalt should pay attention to the influence of asphalt viscosity on the simulation results, and the ultrasonic cavitation intensity is reflected by the volume fraction of cavitation bubbles, so two more The group control simulation is the ultrasonic cavitation simulation of crumb rubber modified asphalt with viscosities of 0.4 Pa·s and 0.8 Pa·s respectively. The points of volume fraction change of cavitation bubbles obtained by ultrasonic cavitation simulation of crumb rubber modified asphalt of three viscosities are shown in Fig.7. It can be seen from the figure that the volume fraction of cavitation bubbles in the three groups of experiments is constantly rising, and there is a process of rising first and then falling in a cycle, and the volume fraction of cavitation bubbles with viscosity of 0.4 Pa·s and 1.2 Pa·s is basically the same in these three cycles. From the beginning of step 200, the volume fraction of cavitation bubbles in the asphalt system with a viscosity of 0.8 Pa·s rises faster than the volume fraction of cavitation bubbles of the other two viscosity asphalt systems, but its cavitation bubble volume fraction also begins to decrease first, therefore, the cavitation bubbles volume fraction of the asphalt system with a

viscosity of 0.8 Pa·s between 470 and 670 steps is lower. As the next cycle progresses, the cavitation bubbles volume fraction of the asphalt system with a viscosity of 0.8 Pa·s will increase again and continue to be higher than that of the other two viscosity asphalt systems, indicating that molten asphalt with a viscosity of 0.8 Pa·s is more conducive to ultrasonic cavitation in the process of ultrasonic powder modification of asphalt.

Fig.7

Influence of ultrasound on the stability of crumb rubber modified asphalt

Asphalt is often in a high temperature state in the storage and transportation stage, so segregation at high temperature will occur. In order to explore the influence of ultrasonic collaborative agitation on the storage of crumb rubber modified asphalt, the storage stability of crumb rubber modified asphalt was evaluated by simulating segregation experiment to test the softening point and the difference of the upper and lower sections. Fig. 8 shows the softening point and difference ($\Delta T_{R\&B}$) of crumb rubber modified asphalt under different control parameters (ultrasonic time is 0min, 5min, 10min, 15min, 20min, 25min) of ultrasonic cooperative mixing process. It can be seen from the figure that the softening point difference of the upper and lower sections of crumb rubber modified asphalt prepared by ultrasonic collaborative stirring process is smaller than that of the upper and lower sections of crumb rubber modified asphalt prepared by pure stirring process, indicating that the collaborative process has a hindering effect on the segregation of crumb rubber. In Fig. 8, the two figures (a) and (b) are the microscopic morphology images taken by the Optical Super Depth-of-Field Microscope (OSM), where (a) is the crumb rubber modified asphalt prepared by only stirring process, and (b) is the crumb rubber modified asphalt prepared by the two processes of ultrasound for 5min and cooperative stirring. Comparing the two figures, it can be seen that after the addition of ultrasonic process, the crumb rubber particles are more refined, indicating that the addition of ultrasonic process can slow down the agglomeration of crumb rubber.

Fig.8

Conclusion

With the assistance of ultrasound, the modified asphalt in the tank is more conducive to moving in the flow field, and its moving speed can reach up to 1.279m/s within the reach of the tool head. Under the action of ultrasound, only positive pressure exists in the modified asphalt flow field after the application of the cavitation model, and the maximum absolute pressure can reach about 1200 kPa, and the change of absolute pressure conforms to the law of periodic motion. Cavitation bubbles are generated under the tool head, and the volume fraction of cavitation bubbles in the tank changes periodically with the change of ultrasound, and with the increase of ultrasonic time, the gas content rate continues to rise, and the cavitation intensity is increasing. With the progress of ultrasound, the general trend of the volume fraction of cavitation bubbles in crumb rubber modified asphalt systems with different viscosities is rising, but it is a process of rising first and then falling in a cycle. in the asphalt system with a viscosity of 0.8 Pa·s, the volume fraction of cavitation bubbles will continue to be higher than that of other viscosity asphalt systems. According to the experimental results, ultrasound process can effectively inhibit the segregation of crumb rubber modified asphalt and slow the agglomeration of crumb rubber modifier.

Nomenclature

u, v, w	the velocity components in the X-axis, Y-axis and Z-axis of the spatial coordinate system are respectively, m/s
ρ	density, kg/m^3
P	pressure, Pa
S_u、S_v、S_w	momentum source components in 3 directions of the X, Y, and Z axes of the spatial coordinate system, N/m^3
μ	dynamic viscosity, Pa·s
λ	second molecular viscosity, Pa·s
T	temperature, ℃
k	fluid heat transfer coefficient, kw/m^2·℃
C_p	specific heat capacity, kj/kg·℃
S_t	sticky dissipative items
x	displacement, m
A	amplitude, μm
f	frequency, Hz
t	time, s
V	velocity, m/s

Acknowledgements

This work was supported by the National Natural Science Foundation of China (Grant No. 51902294), China Postdoctoral Science Foundation (Grant No. 2020M670699), Opening Projects of State Key Laboratory of Special Functional Waterproof Materials (Grant No. SKWL-2021KF31), Graduate Science and Technology Project of North University of China (20231917).

Reference

[1] M. Bueno, M.R. Kakar, Z. Refaa, J. Worlitschek, A. Stamatiou, M.N. Partl, Sci. Rep. 9 (2019) 20342. https://doi.org/10.1038/s41598-019-56808-x

[2] F. Zhang, J.Y. Yu, Constr. Build. Mater. 24 (2010) 410-418. https://doi.org/10.1016/j.conbuildmat.2009.10.003

[3] P.F. Liu, H.N. Xu, D.W. Wang, C.H. Wang, C. Schulze, M. Oeser, Constr. Build. Mater. 162 (2018) 765-780. https://doi.org/10.1016/j.conbuildmat.2017.12.082

[4] M. Zaumanis, L.D. Poulikakos, M.N. Partl, Mater. Des. 141 (2018) 185-201. https://doi.org/10.1016/j.matdes.2017.12.035

[5] E.A.A. Siddig, P.F. Cheng, Y.M. Li, Constr. Build. Mater. 169 (2018) 276-282. https://doi.org/10.1016/j.conbuildmat.2018.03.012

[6] W.Q. Luo, J.C. Chen, Constr. Build. Mater. 25 (2011) 1830-1835. https://doi.org/10.1016/j.conbuildmat.2010.11.079

[7] D. L. Presti. Construct. Build. Mater., 49 (2013) 863-881. https://doi.org/10.1016/j.conbuildmat.2013.09.007

[8] T. Ma, H. Wang, L. He, Y.L. Zhao, X.M. Huang, J. Chen. Mater. Civ. Eng., 29 (2017) 04017036-1-10 https://doi.org/10.1061/(ASCE)MT.1943-5533.0001890

[9] M. Ameri, A. Mansourian, A.H. Sheikhmotevali, Constr. Build. Mater. 40 (2013) 438-447. https://doi.org/10.1016/j.conbuildmat.2012.09.109

[10] O.M. Xu, F.P. Xiao, S. Han, S.N. Amirkhanian, Z.J. Wang, Constr. Build. Mater. 112 (2016) 49-58. https://doi.org/10.1016/j.conbuildmat.2016.02.069

[11] N.Y. Liu, K.Z. Yan, L.Y. You, M. Chen, Constr. Build. Mater. 189 (2018) 460-469. https://doi.org/10.1016/j.conbbuildmat.2018.08.206

[12] Z.L. Jiang, C.B. Hu, S.M. Easa, X.Y. Zheng, Y. Zhang, J. Appl. Polym. Sci. 134 (2017) 44850. https://doi.org/10.1002/app.44850

[13] Z. Leng, R.K. Padhan, A. Sreeram, J. Cleaner Prod. 180 (2018) 682-688. https://doi.org/10.1016/j.jclepro.2018.01.171

[14] X.H. Ding, L.C. Chen, T. Ma, H.X. Ma, L.H. Gu, T. Chen, Y. Ma, Constr. Build. Mater. 203 (2019) 682-688. https://doi.org/10.1016/j.conbuildmat.2019.01.114

[15] J.Y. Hu, T. Ma, T. Yin, Y. Zhou, J. Cleaner Prod. 333 (2022) 130085. https://doi.org/10.1016/j.jclepro.2021.130085

[16] Y.M. Li, R Ma, X.R. Wang, P.F. Cheng, Y.J. Chen. Case Stud. 20 (2024) e02820. https://doi.org/10.1016/j.cscm.2023.e02820

[17] M.M. Phiri, M.J. Phiri, K. Formela, S.P. Hlangothi, Composites, Part B, 204 (2021) 108429. https://doi.org/10.1016/j.compositesb.2020.108429

[18] L. Guo, C.S. Wang, D.J. Lv, D.H. Ren, T.J. Zhai, C.L. Sun, H.C. Liu, J. Cleaner Prod. 279 (2021) 123266. https://doi.org/10.1016/j.jclepro.2020.123266

[19] F. Li, X. Zhang, L.B. Wang, R.X. Zhai, Constr. Build. Mater. 354 (2022) 129168. https://doi.org/10.1016/j.conbuildmat.2022.129168

[20] P.P. Kong, X.H. Chen, G. Xu, W. Wei, Polym. Eng. Sci. 61 (2021) 2567-2575. https://doi.org/10.1002/pen.25783

[21] X. Xiong, Y.M. Chu, Y. Luo, Y. H. Peng, N. N. Yang, J.M. Yan, X. Y. Chen, F. L. Zou, A. Sreeram. J. Cleaner Prod. 426 (2023) 139222. https://doi.org/10.1016/j.jclepro.2023.139222

[22] J.R. Wang, Z.Q. Zhang, Z.L. Li, J. Mater. Civ. Eng. 32 (2019) 04019330. https://doi.org/10.1061/(ASCE)MT.1943-5533.0002971
[23] C. Loderer, M.N. Partl, L.D. Poulikakos, Constr. Build. Mater. 191 (2018) 1159-1171. https://doi.org/10.1016/j.conbuildmat.2018.10.046
[24] D. Özçimen, M.Ö. Gülyurt, B. İnan, Chem. Ind. Chem. Eng. Q. 23 (2017) 367-375. https://doi.org/10.2298/CICEQ160306051O
[25] A. Thakur, R.K. Gupta, V. Udhayabanu, D.R. Peshwe, Y.Y. Mahajan, Philos. Mag. Lett. 103 (2023) 2162617. https://doi.org/10.1080/09500839.2022.2162617
[26] E. Malek, S. Bagherifard, O. Unal, A. Jam, S. Shao, M. Guagliano, N. Shamsaei, Surf. Coat. Technol. 463 (2023) 129512. https://doi.org/10.1016/j.surfcoat.2023.129512
[27] F. Liang, J. Fan, Y.H. Guo, M.H. Fan, J.J. Wang, H.Q. Yang, Ind. Eng. Chem. Res. 47 (2008) 8550-8554. https://doi.org/10.1021/ie8003946
[28] H.T. Kim, H. Shin, I.Y. Jeon, M. Yousaf, J. Baik, H.W. Cheong, N. Park, J.B. Baek, T.H. Kwon, Adv. Mater. 29 (2017) 1702747. https://doi.org/10.1002/adma.201702747
[29] D.P. Mohapatra, D.M. Kirpalani, Appl. Petrochem. Res. 6 (2016) 107-115. https://doi.org/10.1007/s13203-016-0146-1
[30] M. Razavifar, J. Qajar, Chem. Eng. Process.153 (2020) 107964. https://doi.org/10.1016/j.cep.2020.107964
[31] S.M. Mousavi, A. Ramazani, I. Najafi, S.M. Davachi, Petrol. Sci. 9 (2012) 82-88. https://doi.org/10.1007/s12182-012-0186-9
[32] L.M. Wang, Z.K. Song, C. Gong, Case. Stud. Constr. Mat. 16 (2022) e01012. https://doi.org/10.1016/j.cscm.2022.e01012

Figure title

Fig.1. simulation model: (a) Six-blade disc stirrer, (b) Simplified mixed tank model.

Fig.2 Distribution of velocity field in tank when stirring for 2 s

Fig.3 Motion distribution in the mixing tank: (a) The velocity of a point on the tool head, (b) The velocity field distribution in the tank at step 440 of iteration

Fig.4 Pressure changes in the mixing tank: (a) Closing the cavitation model and stirring pressure cloud diagram, (b) The maximum absolute pressure change in the mixing tank

Fig.5 Pressure cloud diagram in mixing tank after iteration of different steps: (a) Iteration step 240, (b) Iteration step 340, (c) Iteration step 440, (d) Iteration step 540 (e) Iteration step 640, (f) Iteration step 740

Fig.6 Variation of the volume fraction of cavitation bubbles in the stirring tank (a) Variation diagram of maximum volume fraction of cavitation bubbles in stirred tank, (b) The Volume fraction distribution of cavitation bubbles in stirring tanks at step 1490 of iteration

Fig.7 The change of volume fraction of cavitation bubbles at 5 mm below the tool head

Fig.8 Segregation experimental results and OSM morphology of crumb rubber modified asphalt under different ultrasonic cooperative mixing process

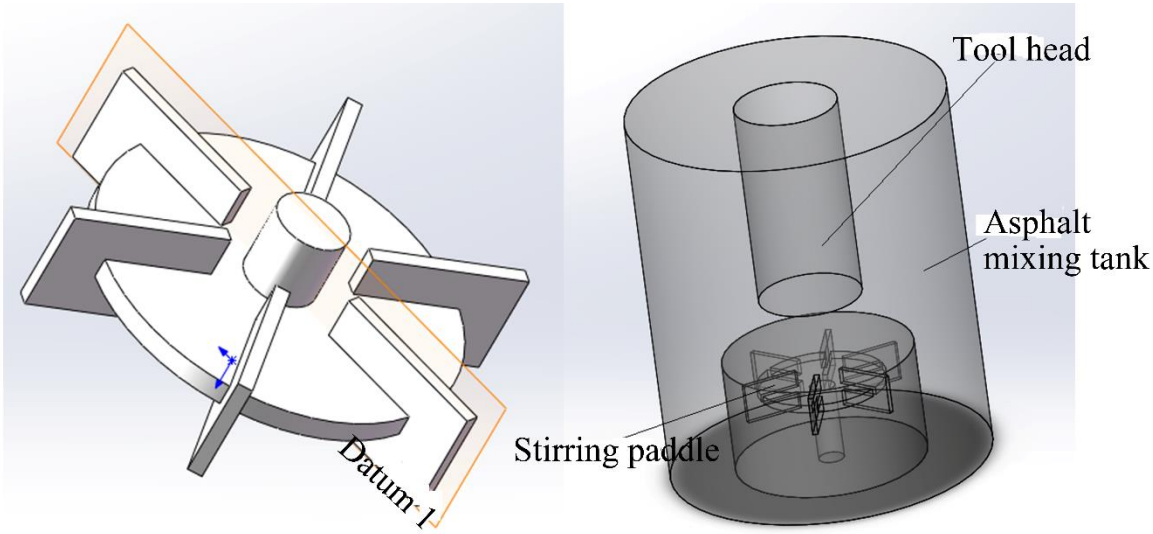
Datum 1
Tool head
Asphalt
mixing tank
Stirring paddle
(a)
(b)

Fig.1

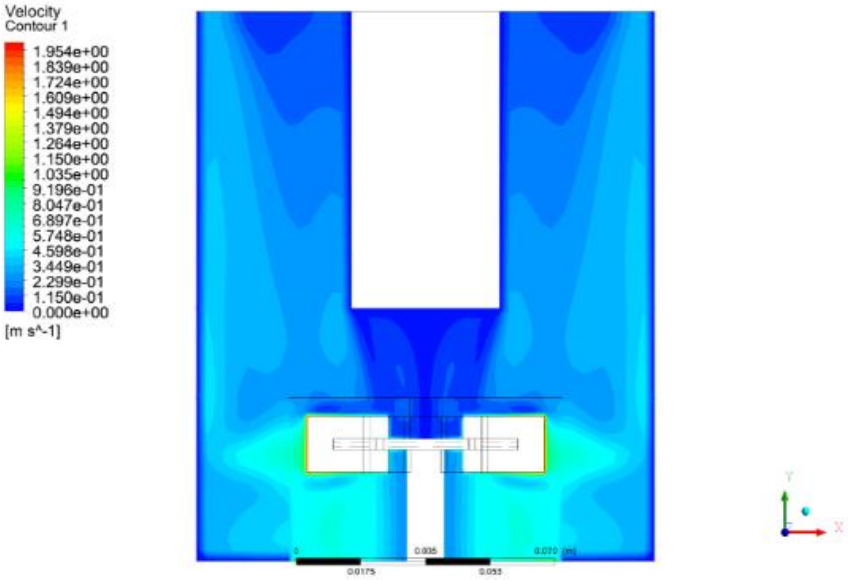
Velocity
Contour 1
1.954e+00
1.839e+00
1.724e+00
1.609e+00
1.494e+00
1.379e+00
1.264e+00
1.150e+00
1.035e+00
9.196e-01
8.047e-01
6.897e-01
5.748e-01
4.598e-01
3.449e-01
2.299e-01
1.150e-01
0.000e+00
[m s^-1]

Fig.2

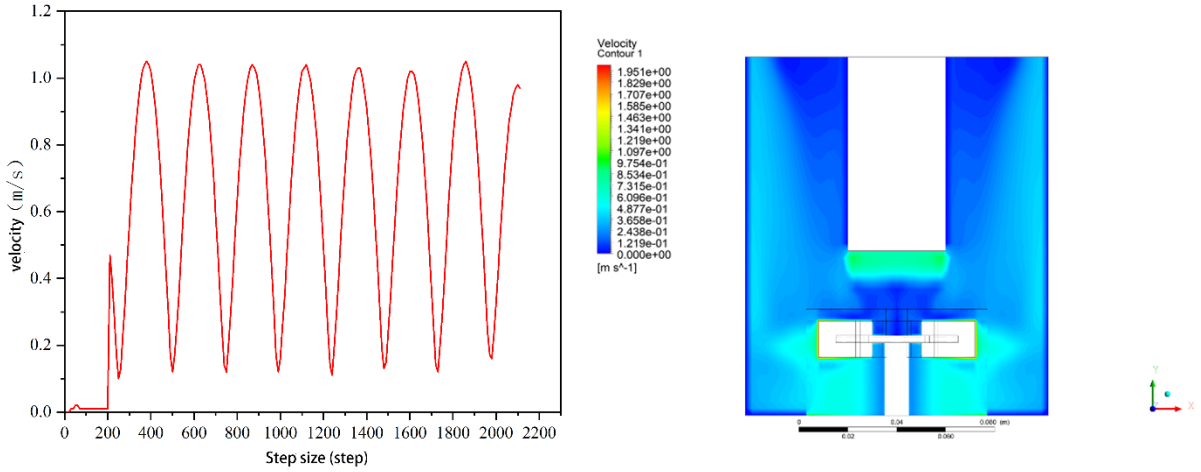

(a) (b)

Fig.3

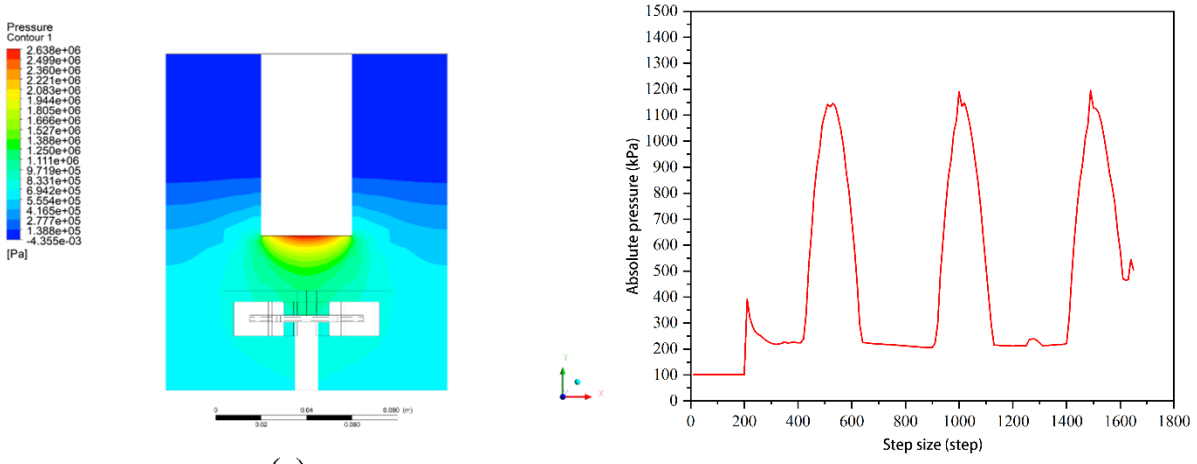

(a) (b)

Fig.4

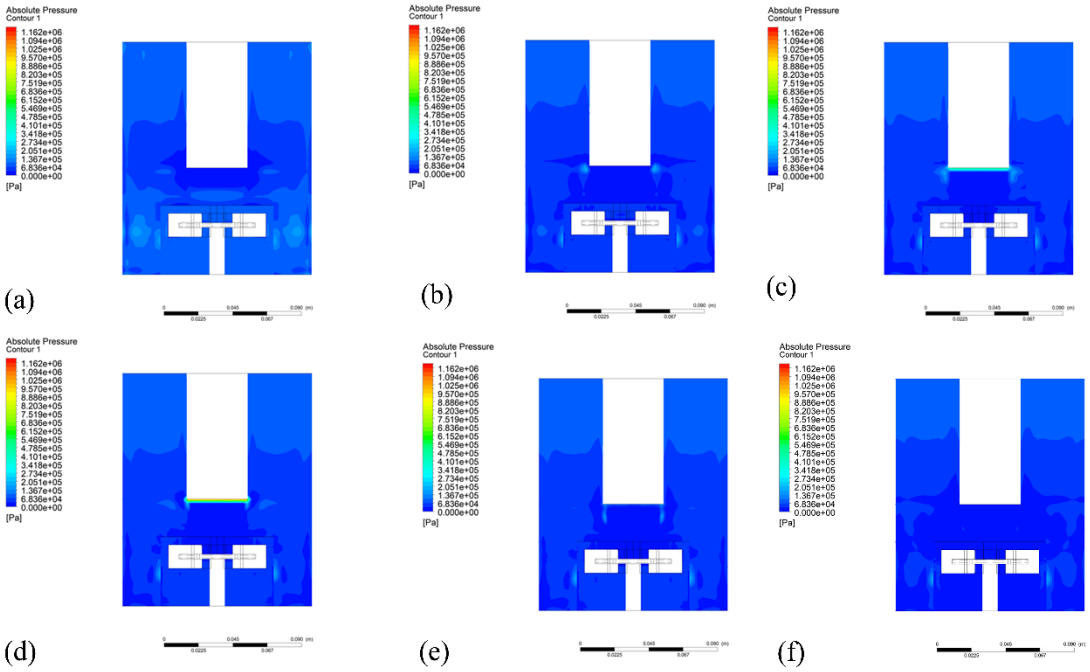
Absolute Pressure
Contour 1
1.162e+06
1.094e+06
1.025e+06
9.570e+05
8.886e+05
8.203e+05
7.519e+05
6.836e+05
6.152e+05
5.469e+05
4.785e+05
4.101e+05
3.418e+05
2.734e+05
2.051e+05
1.367e+05
6.836e+04
0.000e+00
[Pa]
(a)
(b)
(c)
(d)
(e)
(f)

Fig.5

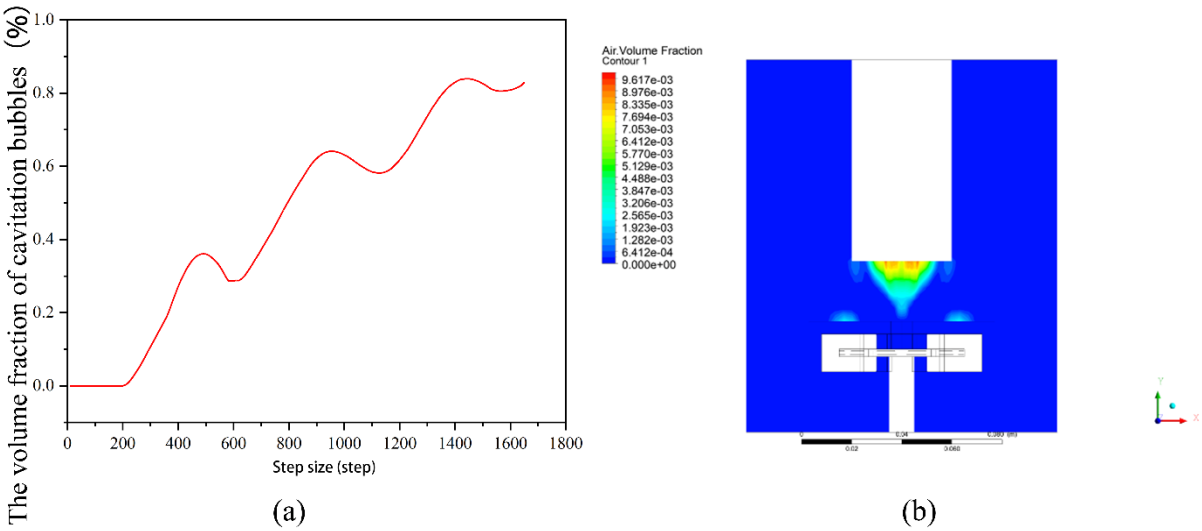
The volume fraction of cavitation bubbles (%)
1.0
0.8
0.6
0.4
0.2
0.0
0
200
400
600
800
1000
1200
1400
1600
1800
Step size (step)
(a)
Air.Volume Fraction
Contour 1
9.617e-03
8.976e-03
8.335e-03
7.694e-03
7.053e-03
6.412e-03
5.770e-03
5.129e-03
4.488e-03
3.847e-03
3.206e-03
2.565e-03
1.923e-03
1.282e-03
6.412e-04
0.000e+00
(b)

Fig.6

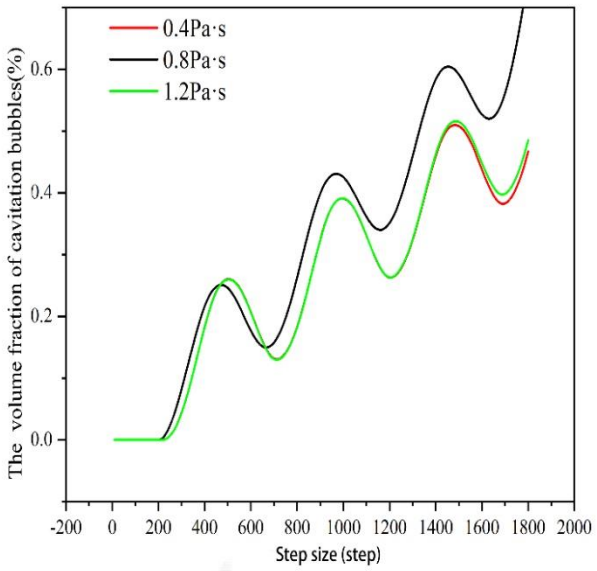
0.4Pa·s
0.8Pa·s
1.2Pa·s
The volume fraction of cavitation bubbles(%)
0.0
0.2
0.4
0.6
-200
0
200
400
600
800
1000
1200
1400
1600
1800
2000
Step size (step)

Fig.7

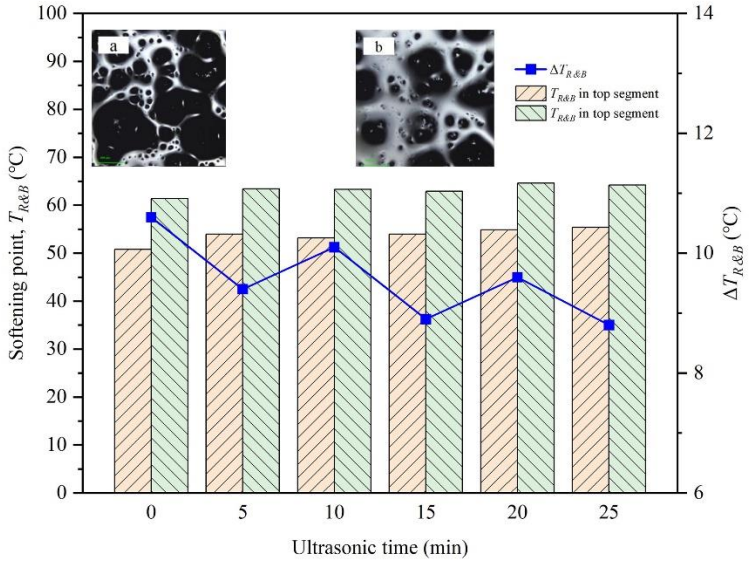
a
b
$\Delta T_{R\&B}$
$T_{R\&B}$ in top segment
$T_{R\&B}$ in top segment
Softening point, $T_{R\&B}$ (°C)
$\Delta T_{R\&B}$ (°C)
Ultrasonic time (min)
0
5
10
15
20
25
6
8
10
12
14

Fig.8